Mechanical Systems and Signal Processing 228 (2025) 112444

Contents lists available at ScienceDirect

Mechanical Systems and Signal Processing

journal homepage: www.elsevier.com/locate/ymssp

Real-time temperature monitoring during titanium alloy machining with cutting tools integrating novel thin-film sensors

Bruno Martins [a,b,*], Carlos Patacas [a,b], Albano Cavaleiro [a,b], Pedro Faia [c], Filipe Fernandes [a,b,d]

[a] IPN - LED&MAT - Instituto Pedro Nunes, Laboratório de Ensaios, Desgaste e Materiais, Rua Pedro Nunes, 3030-199 Coimbra, Portugal
[b] University of Coimbra, CEMMPRE - Centre for Mechanical Engineering Materials and Processes, Department of Mechanical Engineering, Rua Luís Reis Santos, 3030-788 Coimbra, Portugal
[c] University of Coimbra, CEMMPRE – Electrical and Computer Engineering Department, FCTUC, Polo 2, Pinhal de Marrocos, Coimbra 3030-290, Portugal
[d] ISEP - School of Engineering, Polytechnic of Porto, Rua Dr. António Bernardino de Almeida 431, 4200-072 Porto, Portugal

ARTICLE INFO

Communicated by Huei Zhang

Keywords:
Tool condition monitoring (TCM)
Magnetron sputtering
Smart tools
Titanium alloys
Thin-film sensors

ABSTRACT

This study explores the integration of titanium aluminum nitride (TiAlN) and zirconium aluminum nitride (ZrAlN) thin-film sensors into cutting tools for real-time temperature monitoring during machining of Ti6Al4V titanium alloy. These sensors, integrated into a multilayer coating for electrical and wear shielding, were deposited directly onto the tool surfaces and calibrated for temperatures up to 750 °C. Due to the integration into the multilayer coating, the sensors exhibit different β sensitivities across the temperature range, ranging from 108 to 825 K for TiAlN and from 950 to 6681 K for ZrAlN. The cutting tests conducted under various cutting conditions, such as cutting speed, feed rate, depth of cut, and cooling, revealed the influence of these parameters on the cutting temperature. Our findings indicate that the sensor position in the tool's rake face is fundamental for measuring the cutting temperature. The study introduces an innovative tool connector for integration and signal retrieval of the cutting tool in a "plug-and-play" fashion, compatible with industry standards. Additionally, implementing wireless data transmission for real-time and in-situ temperature monitoring offers a pathway for integrating smart cutting tools into modern manufacturing environments, aligning with Industry 4.0.

1. Introduction

Tool condition monitoring (TCM) is essential for the evolution and efficiency of cutting processes, as tool failures account for more than 20 % of machine downtimes [1,2]. Machining efficiency is significantly affected by temperature [3,4] since approximately 90 % of the mechanical energy generated during machining is converted into heat [5], with around 40 % of this heat concentrated at the tool's tip [6]. In particular, the machining of titanium alloys poses significant challenges due to their unique material properties. Titanium is known for its low thermal conductivity and high strength, resulting in high temperatures at the tool-chip interface [5,7–9], often reaching 1000 °C [10]. During titanium machining, the primary mechanisms for heat dissipation – through the workpiece and

* Corresponding author at: IPN - LED&MAT - Instituto Pedro Nunes, Laboratório de Ensaios, Desgaste e Materiais, Rua Pedro Nunes, 3030-199 Coimbra, Portugal.
E-mail address: brunomartins@ipn.pt (B. Martins).

https://doi.org/10.1016/j.ymssp.2025.112444
Received 26 August 2024; Received in revised form 16 January 2025; Accepted 6 February 2025
Available online 18 February 2025

chips – are less effective. Consequently, the high temperatures can lead to rapid tool wear and even catastrophic failure if not correctly managed [3,5,6]. Therefore, monitoring cutting temperatures in real-time is fundamental for optimizing process parameters and ensuring surface quality and better tool life in titanium machining operations.

Advancements in surface engineering extend beyond improving tool wear resistance, providing new thin-film solutions for integrating temperature-sensing capabilities directly into cutting tools. Building on the traditional temperature measurement methods, most research has focused on incorporating thin-film thermocouples (TFTCs) [5,11] to enable real-time thermal monitoring during the machining of titanium alloys. Li et al. [10,12] deposited TFTCs composed of chromel and alumel onto carbide cutting tools using sputtering techniques. They laser-grooved channels on the rake face of the cutting tool to bury the TFTCs, thereby protecting them and ensuring their proximity to the cutting edge (120–200 μm). "Encapsulated" in silicon nitride for electrical shielding, these sensors demonstrated linearity and sensitivity comparable to standard K-type thermocouples (TCs) and effectively measured temperatures during orthogonal dry cutting of titanium, with calibration performed up to 300 °C. Despite these achievements, the studies faced limitations such as inconsistencies in maximum temperature readings (450 °C in the study by Li and colleagues [10] versus 750 °C in another study [12], both considering similar cutting conditions) and the unknown signal response of the TFTCs above 300 °C. Huang et al. [4] employed a similar methodology to validate a simulation model of temperature distribution at the rake face of the tools during the dry turning of titanium. They achieved a maximum temperature of approximately 120 °C with a cutting speed (V_c) of 50 m/min, a feed rate (f) of 0.1 mm/rev, and a depth of cut (a_p) of 0.5 mm. They validated their model and measurements by inserting a standard K-type TC on the cutting tool near the TFTCs, confirming the non-uniform heat flux distribution at the tool-chip interface. However, they did not compare temperatures with previous studies, missing a crucial calibration step.

Li et al. [7] conducted a different approach; they deposited a TFTC using tungsten-26 %rhenium and tungsten-5 %rhenium couples to form a C-type TC on an electrically insulating substrate-type cutting tool. They protected the sensor with an alumina layer and positioned it at 300 μm from the cutting edge. The maximum temperature measured was approximately 130 °C (with $V_c = 90$ m/min, f = 0.1 mm/rev, and $a_p = 0.5$ mm). Like in previous works, the electrical behavior of the sensor above 300 °C remained unknown since calibration was only performed up to this temperature. In a recent study, Lian et al. [6] deposited a TFTC made of NiCr and NiSi on a cutting tool, positioned 100 μm from the cutting edge, for measuring temperatures during the dry cutting of titanium. Their sensor was "encapsulated" within silicon dioxide for electrical and wear protection. The authors calibrated the sensor up to 300 °C and verified its electrical behavior up to 600 °C, above which the coating peeled off. The sensor was validated against thermal imaging and exhibited repeatability and stability, measuring a maximum temperature of 160 °C (for a rotational speed (n) of 570 rev/min, an f = 0.1 mm/rev, and an $a_p = 0.2$ mm). In this case, comparing their temperature measurements with other studies is impractical, as V_c was not specified.

These studies highlight several accomplishments in the field of temperature detection in TCM. The authors successfully deposited TFTCs exhibiting linearity and sensitivity close to the standard TCs on specific cutting tool locations. The sensors demonstrated

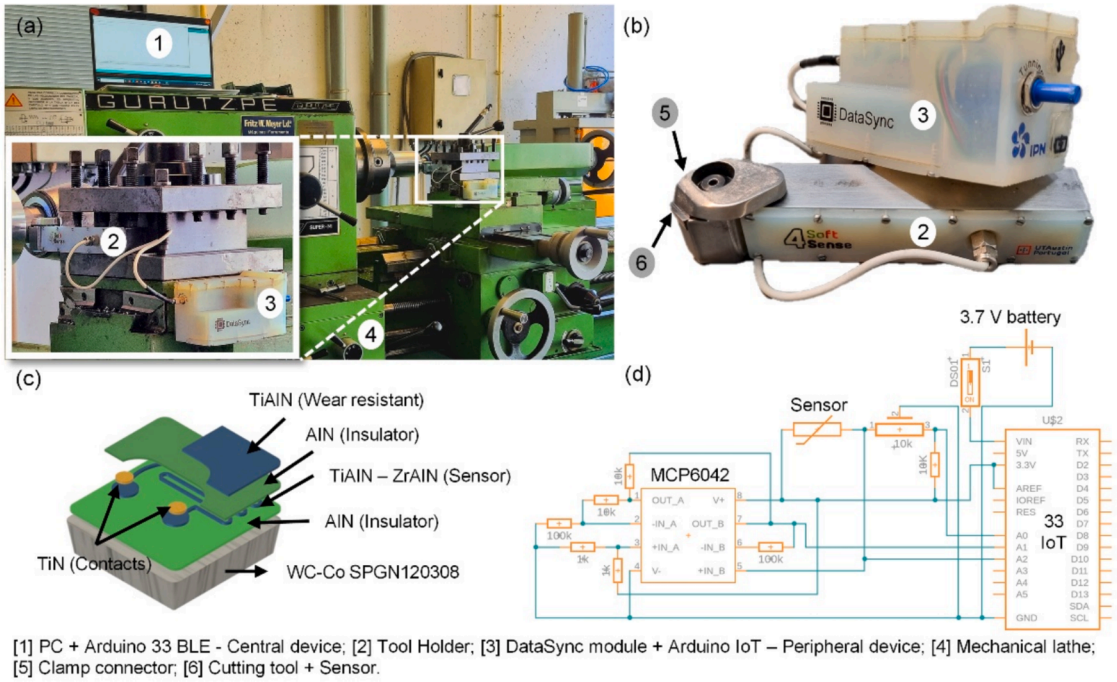

Fig. 1. Experimental setup and schematic for temperature measurement in cutting tools using thin-film thermistors TiAlN and ZrAlN: (a) mechanical lathe Gurutzpe 15 KW with the tool holder (2) DataSync (3) and PC (1); (b) close-up of the tool holder showing the special connector (5) and the cutting tool with the multilayer coating (6); (c) Schematic of the multilayer coating architecture; (d) Electrical schematic illustrating connections to the Arduino Nano 33 IoT board in the DataSync module.

stability and responsiveness under various cutting conditions, enabling real-time temperature measurement during the cutting experiments. However, it is essential to recognize that these approaches are far from industrial integration for several reasons. First, temperature measurements must be more consistent to allow the standardization of these methods [5,13]. Second, most studies employ different deposition techniques for the multilayer coating (sensor protection) and time-consuming patterning techniques (photolithography), making it difficult to scale up the fabrication process. Third, the electrical connections designed for the sensors do not allow interchangeability between tools, meaning each tool must be individually calibrated and cannot be fixed in the tool holder as traditional indexable inserts. Additionally, coolants cannot be used during experiments. To conclude, except for the cutting speed [5,13], which cutting parameter most significantly affects cutting temperature is still unclear.

This work addresses the limitations previously reported in the literature and proposes a solution to bridge the gap between laboratory experiments and industrial integration of TCM by temperature sensing, particularly for cutting titanium alloys. To achieve this, we propose a comprehensive approach that includes the following strategy: (i) employ a full nitride multilayer coating developed in a single magnetron sputtering equipment, incorporating titanium aluminum nitride (TiAlN) and zirconium aluminum nitride (ZrAlN) as temperature sensors, developed in previous studies [14–16]; (ii) calibrate the multilayer coating up to 750 °C, which is essential given the high temperatures typically encountered during the machining of titanium alloys; (iii) utilization of a modified tool holder to retrieve the sensor's signal while maintaining the traditional utility and robustness expected in industrial environments; (iv) execution of orthogonal cutting tests on Ti6Al4V alloys to evaluate the influence of various cutting parameters on temperature, and identify which have the most significant impact on cutting temperatures; (v) investigate the effect of low-pressure cutting fluid on cutting temperatures. As far as we know, this is the first time such an analysis has been conducted using thin-film sensors. Finally, implementing wireless signal transmission using an Arduino platform demonstrates the ease of integrating these thin-film sensors with popular electronics. This aspect of the study aims to validate the system's compatibility with Industry 4.0, showcasing how smart cutting tools can be seamlessly incorporated into modern, automated manufacturing environments.

2. Experimental methods

2.1. Cutting temperature apparatus and sensor calibration

The cutting temperature setup is illustrated in Fig. 1. Fig. 1(a) shows the mechanical lathe Gurutzpe 15 kW equipped with the tool holder (2) and the data acquisition module "DataSync" (3), which transmits temperature data to the PC via Bluetooth (1). Fig. 1(b) provides a close-up of the tool holder, highlighting a special connector (5) designed to retrieve the electrical signal from the cutting tool with the multilayer coating (6) while securely fixing the tool in place. This connector was 3D printed using selective laser sintering (SLS) in 306 stainless steel and was projected to protect the electrical contacts from the harsh cutting environment. The connector allows the cables to pass through inner channels, connecting the cutting tool and the DataSync module. The tool holder CSSPR2525 from SECO® has been modified to accommodate the connector without changing the main characteristics, such as the positive rake orthogonal angle (5), cutting edge angle (45), and global dimensions. This design also enables the tool holder to be handled according to industrial practice, maintaining the "plug-and-play" system for the cutting tool insert.

In Fig. 1(c), the ZrAlN and TiAlN active layers are "sandwiched" between aluminum nitride (AlN) insulator films, exhibiting thicknesses of 1000 nm and 600 nm, respectively, and the entire structure is coated with TiAlN to improve wear resistance. The multilayer coating was applied using a single magnetron sputtering unit with four sputtering targets arranged in a closed-field magnetic configuration – two targets of zirconium/titanium and two of aluminum. The detailed process steps and parameters, except those of the ZrAlN layer, were already depicted in the literature [16]. A resume of the deposition parameters for the ZrAlN layer is provided in Table 1.

The multilayer coating's electrical resistance variation due to temperature changes was evaluated using the two-point measurement (2PM) method. The calibration process involved four temperature cycles from ambient temperature to 750 °C with heating rates of about 20 °C/minute and natural cooling. The electrical resistance was recorded with a high-resolution multimeter (acquisition frequency of 10 Hz), while the obtained data fitting was done using Eq. (1), considering the resistance value at room temperature

Table 1
Deposition conditions for the deposition of the ZrAlN sensor layer within the multilayer coating.

Deposition parameters	
Gas mixture ratio (N_2/Ar)	1.6
Working pressure (Pa)	≈ 0.25
Table speed (RPM)	1
Satellite speed (RPM)	5
Al Power density (W·cm^{-2})	≈ 1.9 (x2)
Zr Power density (W·cm^{-2})	≈ 5.5 (x2)
Substrate bias (V)	−40
Bias pulse frequency (kHz)	250
Bias reverse time (μs)	0.5
Deposition time (min)	60
Target-substrate distance (mm)	100
Substrate temperature (°C)	≈ 200

(R25). Calibration was performed under vacuum in an Ar/5%H_2 atmosphere to prevent oxidation of the titanium nitride (TiN) contacts and of the tungsten carbide (WC) substrate, ensuring operational stability and performance of the sensor's layer within the multilayer architecture. The index β or thermistor sensitivity over a defined temperature range (50–200 °C) was derived with:

$$\beta_{[50-200\,^\circ C]} = \frac{\ln\left(\frac{R_{T1}}{R_{T2}}\right)}{\left(\frac{1}{T_1} - \frac{1}{T_2}\right)} \quad (1)$$

In Eq. (1), β is in K, and R_{T1} and R_{T2} represent the electrical resistance at temperatures T_1 and T_2.

The electrical schematic (see Fig. 1(d)) presents the connections to the Arduino Nano 33 IoT (33IoT) board, housed in the DataSync module, to transmit temperature data to the Arduino Nano 33 BLE (33BLE) via Bluetooth®, connected to the PC (1). The 33IoT board was set as a peripheral device, while the 33BLE was set as a central device. The diagram shows the connections between the 33IoT, the operational amplifier (Op Amp) – Microchip® Rail-to-Rail Input/Output MCP6042 for signal amplification – and a 10 kΩ variable resistor for setpoint tuning of the TiAlN system. Previous studies have confirmed that the TiAlN system has a lower β value than the ZrAlN [14–16], which requires signal amplification. Resistors were set to amplify approximately ten times, and a 3.7 V battery was included to power the electronic system. Temperature acquisition was performed through a voltage divider between the sensor and the 10 kΩ variable resistor. The temperature (T) in K was computed using Eq. (2):

$$T = \frac{RT \cdot \beta}{\left(RT \cdot \log\frac{Rsensor}{R25} + \beta\right)} \quad (2)$$

In Eq. (2), RT represents the temperature at room temperature in K, Rsensor represents the sensor's resistance in Ω, and R25 stands for the resistance at room temperature, also in Ω. The thermistor sensitivity β is calculated by Eq. (1). Eq. (2) was coded (C ++) in the Arduino integrated development environment (IDE) to return the temperature measured with the cutting tool.

Two Arduino analog input ports were used to address variability in R25 among tools [16]. Analog A0 measures the voltage from the voltage divider between the 10 kΩ variable resistor and an internal 10 kΩ resistor (set as a constant variable in the IDE), storing the resistance value of the variable resistor. Analog A2 measures the voltage from the voltage divider between the sensor and the variable resistor (pre-stored value). This configuration allows automatic computation and storage of R25 when the sensor is connected, ensuring correct temperature readings. R25 should closely match Rsensor at room temperature in Eq. (2). Analog input A1 reads the voltage from the OpAmp for the TiAlN sensor to retrieve the sensor resistance, and it is not used when the ZrAlN sensor is connected. Following the calibration, the operational stability and accuracy of the multilayer coating were further tested at constant temperatures of 100 and 200 °C for 10 min in vacuum to verify the accuracy and reliability of the Bluetooth signal, specifically for the TiAlN sensor. An acquisition rate of 100 ms was used for all experiments.

2.2. Cutting conditions for turning Ti6Al4V alloy and surface analysis

The cutting tests were conducted on a titanium alloy workpiece measuring 55 mm long and 80 mm in diameter. The cutting parameters were selected based on the conditions recommended by SECO® for the SPGN120308 CP200 tool with a nose radius of 0.8 mm: cutting speed (Vc) – 25 to 44 m/min; feed rate (f) – 0.21 to 0.39 mm/rev; depth of cut (a_p) – 0.21 to 1.93 mm. The initial cut was performed with a cutting speed of 35 m/min, a feed rate of 0.12 mm/rev, and a depth of cut of 1 mm. This cut was intended to verify the system's response by making six tiny grooves, each 3 mm long and 0.3 mm deep, into the workpiece with an approximate spacing of 5 mm between them. Table 2 presents the cutting conditions used for machining the titanium alloy. Conditions 1 to 3 focused on testing the effect of varying the depth of cut, while conditions 1 to 6 evaluated the impact of different feed rates. Conditions 6, 7, and 8 further examined the effect of the depth of cut, and condition 9 investigated the influence of mild cooling on the cutting edge. The cutting coolant used was the Castrol® Almaredge 230 K, a soluble fluid for metalworking with a 6 % concentration in water. Finally, conditions 1 and 10 were compared to assess the effect of cutting speed. These experiments were initially performed with the TiAlN

Table 2
Cutting conditions for cutting Ti6Al4V alloy.

Condition	f (mm/rev)	a_p (mm)	Average V_c (m/min)
1	0.293	1.0	41
2		1.25	
3		1.5	
4	0.421	1.0	
5		1.25	
6		1.5	
7		1.75	
8		2.0	
9		2.0	
10	0.293	1.0	80

sensor.

Testing conditions 3, 6, and 8 were subsequently repeated with the ZrAlN sensor to assess its repeatability. The performance of TiAlN and ZrAlN sensors was also compared using testing conditions 8. The rotational speed (n) of the lathe was calculated using the following equation:

$$n = \frac{V_c \cdot 1000}{(\pi \cdot D)} \tag{3}$$

In Eq. (3), n is in rpm, V_c is m/min, and D represents the diameter of the workpiece in mm.

The surface topography of the rake face of the tools, close to the cutting edge, was analyzed using a confocal microscope (Infinite Focus from Alicona), which provides detailed surface profiles. This analysis was performed before and after the cutting experiments on the tool equipped with the TiAlN sensor. A comparative analysis was also conducted on the ZrAlN sensor tool to assess differences in surface degradation.

3. Results and discussion

3.1. TiAlN and ZrAlN sensor's calibration

The calibration of the ZrAlN and TiAlN sensors ensures accurate temperature measurements during the cutting experiments. Fig. 2 provides an overview of the sensor positioning, design, and high-temperature calibration setup. Fig. 2(a) and (c) illustrate the cutting tool coated with the multilayer coating according to the architecture shown in Fig. 1(c) for the TiAlN and ZrAlN sensors, respectively. Fig. 2(a) also displays the positioning of the cutting tool in the tool holder. Fig. 2(b) and (d) depict the positions of the TiAlN and ZrAlN sensors on the rake face of the cutting tool, respectively. Both sensors were positioned at 1 mm of the cutting edge, which is the minimum distance to avoid the detachment of polyimide tape (used as a shadow mask) during the deposition of the sensor [16]. The sensor design differs for each material: the TiAlN sensor has a meander structure, while the ZrAlN sensor has a simple square design. The higher resistivity of ZrAlN compared to TiAlN [14,15] means that a meander structure would unnecessarily increase the sensor's resistance and acquisition system complexity. Additionally, the location of the TiN contacts aligns with the copper spring-load pins inserted in the connector (see Fig. 1(b) label 5), ensuring a perfect contact when fixing the cutting tool. Fig. 2(e) presents a close-up of the calibration experiment conducted up to 750 °C in a vacuum environment with an Ar/5%H_2 reducing atmosphere, simulating the temperature conditions during cutting operations.

3.2. Sensor's performance and temperature sensitivity

Fig. 3 shows the logarithm of resistance response to temperature of the cutting tool coated with the multilayer coating containing TiAlN (Fig. 3(a)) and ZrAlN (Fig. 3(b)) as temperature sensors. Both cutting tools underwent thermal annealing for 20 min at 400 °C in

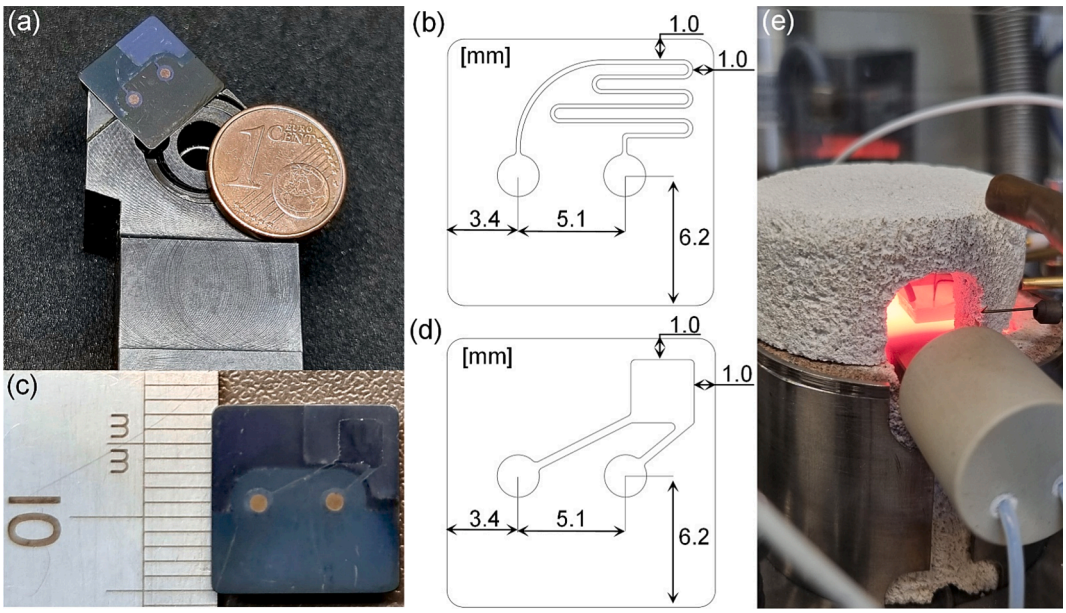

Fig. 2. TiAlN and ZrAlN sensor design and testing: (a) position of the cutting tool in the tool holder; (b) position of the TiAlN sensor on the tool's rake face; (c) cutting tool with the ZrAlN sensor embedded; (d) position of the ZrAlN sensor on the tool's rake face; (e) Close-up of the calibration experiment up to 750 °C in a vacuum with Ar/5%H_2 as the reducing atmosphere.

vacuum, in line with the strategy outlined in a recent study [16]. As expected, both sensors exhibit semiconductor behavior, decreasing resistance as temperature increases. The calculated sensitivity β is 108.1 K and 951.8 K for the TiAlN and ZrAlN layers, respectively, consistent with values reported in the literature for these films [15,16]. While semiconductor behavior and sensitivity values align with expectations and previous studies, we acknowledge a limitation in our methodology related to the stabilization procedure. The annealing temperature of 400 °C, although optimal based on previous studies [16], is significantly lower than the calibration temperatures, which reach up to 750 °C. Although the sensors recover to their initial resistance after the cycling tests, suggesting stability under brief high-temperature exposures, further research is necessary to determine if this stability is maintained under prolonged exposure at high temperatures.

The β fit for the TiAlN sensor aligns well with the average values measured up to 400 °C (see Fig. 3(a)). However, above 400 °C, the resistance deviates significantly from the fitting, showing a marked decrease. This alignment between the fit and measured values up to 400 °C is also reported in a prior study where the same multilayer coating embedded with TiAlN was investigated as a temperature sensor [16].

Considering the ZrAlN sensor (see Fig. 3(b)), a similar behavior is observed, although the β fit starts to deviate slightly above 300 °C. It is important to note that both sensors exhibit similar responses and repeatability but are somewhat complex to calibrate. Above 400 °C, there is a sharp increase in sensitivity, with the TiAlN and ZrAlN showing sensitivities (400–600 °C range) of 825.2 ± 110.3 K and 6681.8 ± 496.5 K, respectively. Notably, the multilayer coating with the ZrAlN sensor shows sensitivities that compete with traditional thermistors at the highest temperatures [17].

Two possible explanations exist for this unexpected decrease in resistance above the 400 °C threshold. One possibility is the self-heating effect found in thermistors, which promotes a reduction in resistivity due to Joule heating from the passing current [18,19]. Another plausible explanation is the influence of the AlN insulator in the multilayer coating. AlN films, known for their dielectric properties, often exhibit conduction governed by the Poole-Frenkel effect [20,21]. As temperature increases, it becomes easier for charge carriers trapped in defects to gain enough energy to move into the conduction band, increasing leakage current. A recent study has shown multilayer coatings, including AlN insulation layers, containing typical sputtering growth defects such as voids and droplets [16]. Additionally, traditional thin-film insulation materials like aluminum oxide are known to lose insulation resistance with temperature [22]. Since the TiAlN sensor as a single layer does not exhibit the behavior observed in Fig. 3(a), as reported by Martins et al. [16], it is assumed that the second explanation is the valid one to clarify the response of the multilayer coating. This suggests that the insulator material plays a significant role in the calibration and performance of the sensor layer at higher temperatures.

3.3. *Stability analysis using Arduino as the data acquisition system*

Given the results presented in Fig. 3, developing a calibration model to cover the entire temperature range would require a combination of β values for different segments or a non-linear fit using a polynomial or exponential equation. As mentioned, R25 varies slightly within the same material and significantly between TiAlN and ZrAlN. This would necessitate a complex calibration strategy beyond the scope of our study. Since the beta fit is suitable up to 400 °C, we utilized it as the calibration model for both sensors in Eq. (2) in the Arduino IDE.

Considering the 12-bit analog-to-digital converter of the Arduino, the resolution of the TiAlN sensor is approximately 0.2 °C/step with the amplification, while the ZrAlN sensor achieves roughly a 0.3 °C/step without amplification. Fig. 4 shows the temperature response for the multilayer coating with TiAlN sensor using the 33IoT board as the acquisition system. The tests evaluated signal stability and cycling performance from 300 to 400 °C. In both Fig. 4(a) and (b), it is possible to observe the tuning of the signal to match the temperature given by the reference thermocouple (TC) at the beginning of the experiment. Fig. 4(a) shows the temperature

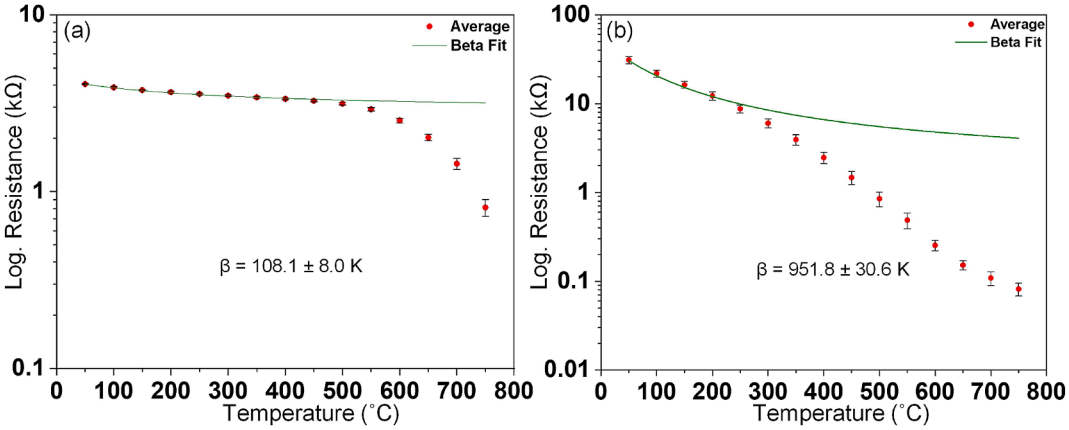

Fig. 3. Calibration of TiAlN and ZrAlN sensors deposited on the cutting tool: (a) average and β fit calculated after four heating–cooling experiments up to 750 °C with TiAlN as the temperature sensor; b) average and β fit calculated after four heating–cooling experiments up to 750 °C with ZrAlN as the temperature sensor.

response during a single heating–cooling cycle with holding steps at 100 and 200 °C for approximately 10 min each. The temperature measured by the TiAlN sensor closely follows the TC, demonstrating good agreement and stability. The sensor's error is close to 8 % at 100 °C and 3.5 % at 200 °C, slightly lower than the error already reported in the literature [16] for the same system. Though small, these deviations can be attributed to the initial tuning executed while utilizing the β function for the calibration. The Fig. 4(b) illustrates the temperature response during multiple heating–cooling cycles, ranging from 300 to 400 °C. The sensor's performance remains consistent across the cycles, maintaining close alignment with the TC and sustaining accuracy and stability over repeated cycles.

The overall trend indicates that the complete system can accurately track temperature changes, providing reliable data throughout the cycles. The close match with the TC validates the sensor's accuracy and reliability. The slight lag observed in Fig. 4(b) results from thermal inertia and likely differences in sensor response times: 8.3 s for the thermocouple and 9.3 s for the thin-film sensor.

During the cooling steps, it is visible that the TC shows a faster temperature decrease. These results highlight the efficacy of the calibration, using the β function, up to 400 °C, which was used for both sensors during the cutting experiments.

3.4. Cutting temperature with TiAlN as temperature sensor

Fig. 5 presents the temperature profile recorded during the first cutting test on a titanium alloy workpiece using the TiAlN sensor while using the device depicted in Fig. 1. The figure captures the thermal dynamics, highlighting critical phases of the cutting process. At the onset of the cutting operation, the tool contacts the workpiece material, initiating a rapid increase in temperature. This initial rise is attributed to the friction and plastic deformation at the tool-workpiece interface. The temperature immediately increases to around 80–100 °C, after which the increase slows down, indicating a quasi-steady-state condition. In this phase, although the temperature continues to rise, the slope of the temperature curve is significantly lower compared to the initial stage, suggesting that the heat generation and dissipation rates are close to equilibrium but have not fully stabilized. This temperature response during the cutting of titanium alloys has already been depicted in the literature [4,6,9,10]. The periodic temperature fluctuations correspond to the passage of the tool over the tiny grooves indented in the workpiece surface, briefly reducing the a_p. This intermittent behavior demonstrates the sensor's sensitivity to subtle changes in the cutting environment. A rapid temperature decrease is observed as the tool retracts from the workpiece for around 300 s. This drop reflects the interruption of frictional heating and the dissipation of residual heat through the cutting tool, tool holder, and surrounding environment. The sensor's fast response during this phase further validates its capability for real-time temperature monitoring.

The general understanding is that titanium cutting develops at high temperatures [5,10]. However, as discussed in the introduction, it is challenging to directly compare the temperatures measured in this study with those reported in the literature. For instance, high cutting speeds (80–90 m/min) can yield temperatures ranging from as low as 130 °C [7] to as high as 750 °C [12]. Several factors can contribute to these discrepancies, including differences in cutting equipment, sensor distance relative to the cutting edge, sensor stability, and tool rigidity. In this study, it is believed that the distance of the sensor from the cutting edge plays a significant role in the measured temperatures. Our sensors were positioned approximately 1 mm from the cutting edge to avoid detachment issues of the shadow masks during deposition. While necessary for sensor patterning, this positioning may result in lower temperature readings than sensors closer to the cutting edge. Furthermore, there is a strong consensus that the highest temperatures are developed at the cutting edge, specifically within the primary and secondary deformation zone [4] of the tool-workpiece interface, typically at distances below 0.5 mm [3,6,9,23]. This zone experiences the most intense friction and plastic deformation, leading to peak temperatures that the current sensor positioning might not fully capture.

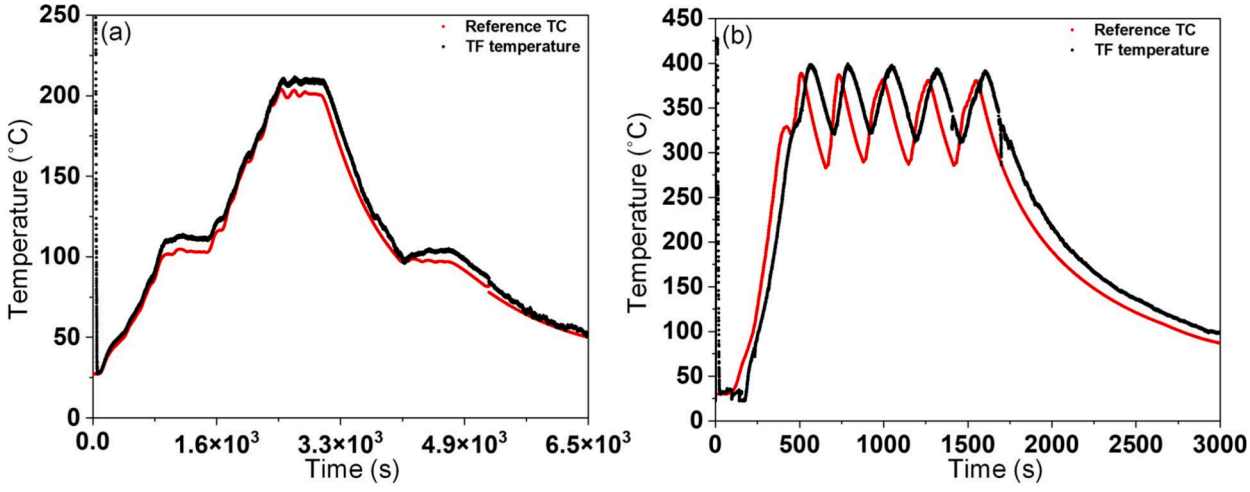

Fig. 4. Heating-cooling testing of the multilayer coating with TiAlN as sensor and the Arduino board as the acquisition system in vacuum: (a) signal stability evaluation at 100 and 200 °C; (b) cycling tests from 300 to 400 °C.

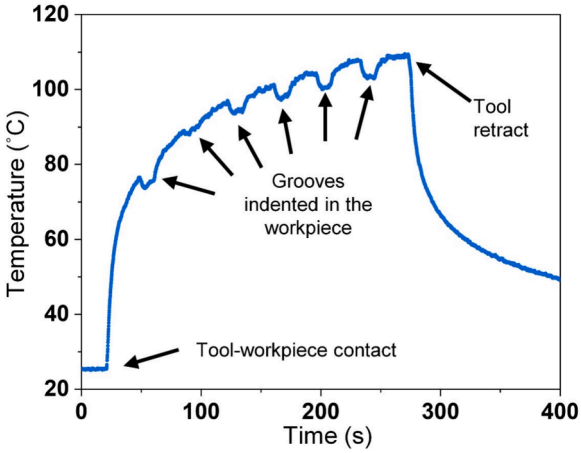

Fig. 5. First cutting test on the titanium alloy with tiny grooves created in the workpiece surface: cutting conditions; $V_c = 35$ m/min, f = 0.12 mm/rev, $a_p = 1$ mm.

3.5. Cutting parameters and their impact on cutting temperature

Fig. 6 presents temperature measurements made during the cutting of the titanium alloy with the TiAlN sensor under various cutting conditions, as detailed in Table 2. Particularly, it illustrates the impact of different cutting parameters on the measured temperatures close to the tool-workpiece interface. The experiments were designed to assess the effects of feed rate, depth of cut, cutting speed, and low-pressure cooling on the cutting temperature. In Fig. 6(a), the temperature profiles are shown for varying feed

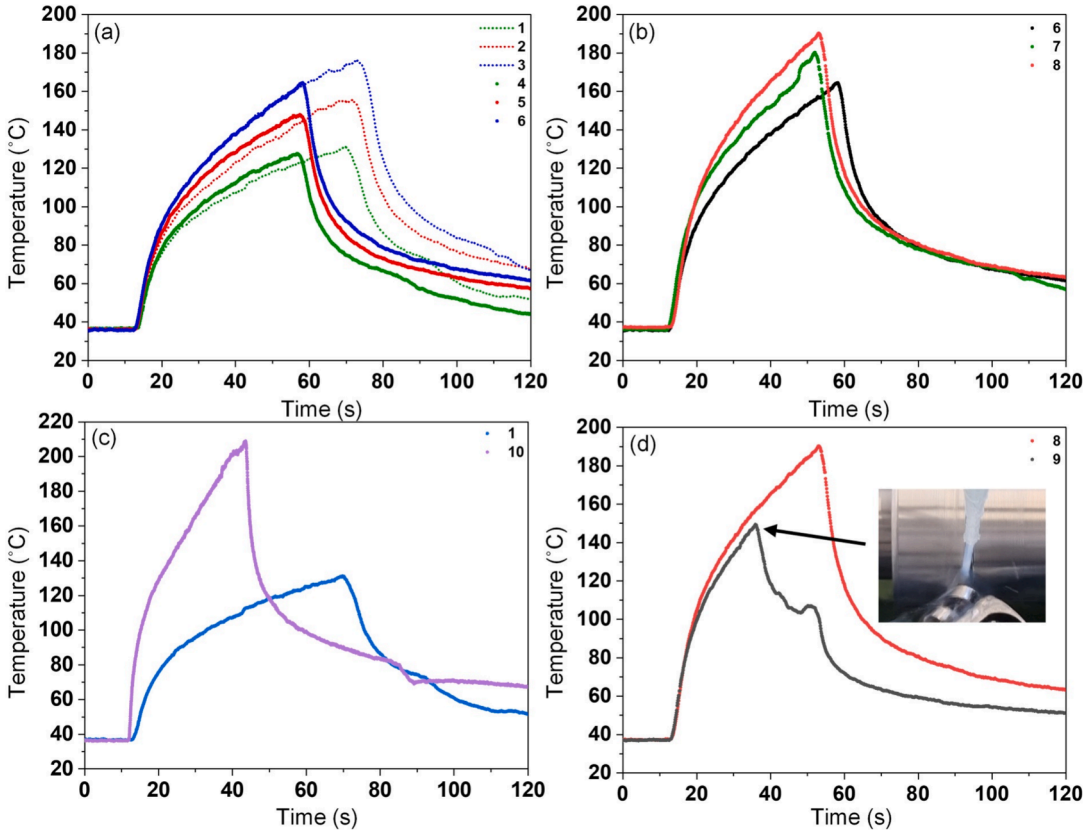

Fig. 6. Temperature measurements during the cutting of titanium alloy with different cutting conditions, using the TiAlN as a sensor: (a) temperature profile with different a_p and f; (b) temperature profile with different a_p; (c) temperature profile with different V_c; (d) temperature profile comparing dry and under cooling conditions. The cutting experiments correspond to the conditions depicted in Table 2.

rates (f) and depths of cut (a_p). Experiments 1 to 3 demonstrate how increasing the depth of cut from 1.0 mm to 1.5 mm at a constant feed rate (f = 0.293 mm/rev) results in higher temperatures. This increase in temperature can be attributed to the larger volume of material being cut, which generates more frictional heat [5,6,8]. Experiments 4 to 6 compare the effect of increasing the feed rate from 0.293 mm/rev to 0.421 mm/rev while maintaining the same range of depths of cut. Interestingly, the temperature profiles for the same a_p are similar across the different feed rates. This observation suggests that feed rate may not significantly impact the cutting temperature as the depth of cut does, reducing the overall machining time [3,6,7].

Fig. 6(b) focuses on the effect of varying the depth of cut while keeping the feed rate constant (f = 0.421 mm/rev). Experiments 6 to 8 show the temperature profiles for depths of cut from 1.5 mm to 2.0 mm. As expected, higher depths of cut result in higher temperatures, which agrees with the results from Fig. 6(a). This is consistent with the understanding that greater cutting forces and more material deformation led to increased frictional heating [3,5,7]. The similarity in the general shape of the temperature curves across these experiments suggests a predictable relationship between the depth of cut and cutting temperature, validating the importance of optimizing a_p for temperature control [6,7]. Fig. 6(c) compares the temperature profiles at two different cutting speeds: experiment 1 (V_c = 41 m/min) and experiment 10 (V_c = 80 m/min) demonstrate that increased cutting speed results in higher temperatures, as expected [3]. The higher cutting speed reduces the time available for heat dissipation, leading to higher thermal loads at the cutting edge [5–7]. These experiments emphasize the need for the careful consideration of cutting speed and depth of cut parameters since doubling V_c or a_p results in a 60 and 46 % increase in cutting temperature, respectively; on the other hand, increasing the feed rate by 1.5 times only impacts the temperature by about 7 %.

Fig. 6(d) illustrates the impact of cooling conditions on the cutting temperature. The cutting experiment video can be found in the Supplementary Material. Experiments 8 (dry cutting) and 9 (cutting with cooling) reveal the effectiveness of cooling in reducing cutting temperatures. The temperature peak during dry cutting reaches approximately 190 °C, whereas using cooling significantly lowers the temperature to about 110 °C. These results suggest that the contribution of the cooling in the temperature is more effective than reducing the cutting speed or the depth of cut [5,8].

3.6. Cutting temperature with ZrAlN as temperature sensor

Fig. 7 presents the temperature measurements during the cutting of titanium alloy using the ZrAlN film sensor under various cutting conditions, as detailed in Table 2. These experiments aimed to assess the ZrAlN performance by monitoring the cutting temperature in real-time and demonstrating the feasibility of changing the cutting tools. One of the advancements highlighted by this study is the "plug-and-play" capability of the cutting tools equipped with thin-film sensors, representing a novel achievement in the cutting field. The cutting tools could be used interchangeably without requiring extensive recalibration or modifications by updating the beta sensitivity corresponding to the ZrAlN sensor in the Arduino code. This approach bridges the gap between the laboratory and industrial requirements by simplifying the process of tool replacement.

Fig. 7(a) illustrates the temperature profiles obtained for tests 1, 2, and 3, conducted under the same cutting conditions, specifically, conditions 3 in Table 2. These tests primarily focused on evaluating the repeatability of temperature measurements using the ZrAlN sensor under identical cutting conditions. The temperature profiles for these experiments reveal a similar pattern characterized by an initial rapid rise in temperature, reaching a peak and declining as the tool retracts from the workpiece. This pattern follows the same behavior observed in Fig. 6 for the TiAlN sensor. It is essential to note the differences in the temperature curve towards the end of the test, especially for test 3. Since the tool holder has a cutting-edge angle of 45°, when the cutting tool approaches the lathe chuck, it leaves a 45° angle section as the workpiece progressively decreases in diameter. This means that subsequent cuts face a sudden change in depth of cut if the tool holder is not instantly retracted. The inset in Fig. 7(a) shows this event, where a large chip and the corresponding peak in the temperature curve can be observed. This behavior further acknowledges the effect of the depth of cut in the

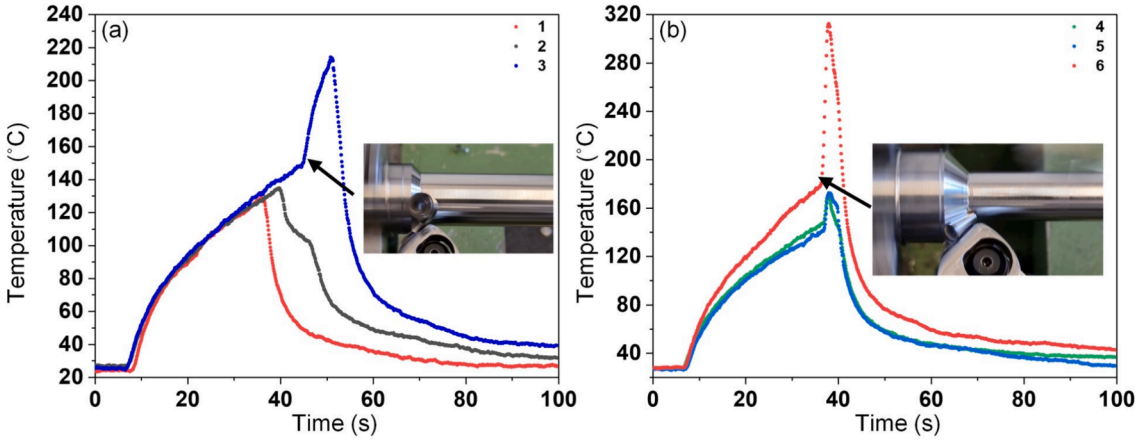

Fig. 7. Temperature measurements during the cutting of titanium alloy with different cutting conditions, using the TiAlN as sensor: (a) tests 1,2 and 3 using cutting conditions 3; (b) tests 4 and 5 using cutting conditions 6, and test 6 using cutting conditions 8, Table 2.

cutting temperature. This figure discloses another variable to consider in cutting operations, especially while turning: cutting time. Since a steady state is not observed, the cutting temperature increases with cutting time, going from 128 to 150 °C in 10 s.

Fig. 7(b) presents the temperature profiles for cutting tests 4 and 5, using conditions 6 and cutting test 6, using conditions 8 (see Table 2). Tests 4 and 5 show similarities between the temperature curves under the same cutting conditions, as observed in curves 1, 2, and 3 of Fig. 7(a). The similarity between temperature curves across these tests emphasizes the ZrAlN sensor system's repeatability and suggests that the sensors provide consistent temperature measurements, irrespective of the slight variations in the cutting environment or tool positioning. This conclusion is supported by the temperature peak at the end of test 6. The inset of Fig. 7(b) shows the tool approaching the lathe chuck with a chip exhibiting a large width due to the sudden change in depth of cut for the reasons previously explained. The peak temperature at almost 320 °C highlights the sensor's fast response. The cutting test video can be checked in the Supplementary Material.

3.7. Sensor's comparative analysis

Fig. 8 compares temperature profiles obtained for TiAlN and ZrAlN sensors under the same cutting conditions. The conditions depicted are 6 and 8 (see Table 2) for the bottom and upper plots, respectively. This comparison highlights the similarities between the sensors in real-time temperature monitoring during the cutting of titanium alloy. Both sensors exhibit similar temperature curve shapes when cutting under the same conditions, indicating a reliable calibration procedure. However, there is a gap between the maximum temperatures measured by the two sensors, with the TiAlN sensor recording a higher peak temperature of approximately 15 °C. This minor difference can be attributed to several factors: firstly, using the β function as a calibration curve might be better suited to the TiAlN sensor; secondly, the manual placement of the shadow masks for the sensor deposition process [16] could introduce slight positional deviations and affect the sensor's exact location on the tool's rake face, leading to minor differences in temperature measurements; thirdly, the sensor's design may contribute to the observed differences. The TiAlN sensor features a meander design, which could offer a more even temperature distribution along the cutting edge.

Finally, these results suggest that both sensors can capture the essential thermal dynamics of the cutting process. Each sensor exhibits distinct advantages and disadvantages that must be carefully considered when selecting the appropriate sensor for specific applications. The ZrAlN sensor demonstrates superior sensitivity compared to the TiAlN one, eliminating the need for signal amplification and simplifying the overall electronics design. However, the beta function calibration process appears to fit the TiAlN sensor better, potentially resulting in lower measurement errors, especially at temperatures above 300 °C. Furthermore, the higher resistivity of the ZrAlN sensor supports simpler sensor designs, though it may return sensors with high electrical resistance.

3.8. Tool's surface topography and post-cutting wear analysis

Fig. 9 provides a detailed analysis of the surface topography of the rake face of the cutting tool, particularly close to the cutting edge. The central image displays a 3D topographical map of the rake face, with the color scale on the left indicating height variations across the surface. The arrows highlight specific regions of interest where it is possible to determine the x and y distances from the cutting edge through the 2D inset profiles. The detailed 3D surface colored profile clearly shows the sensor location throughout the rake surface of the tool, corresponding to the orange color index.

The lower left inset depicts the 2D surface profile along the specific line on the rake face, showing the surface height variation along the x-axis. The vertical red line indicates a transition in the surface corresponding to the sensor edge, while the sharp decline corresponds to the tool's edge. The x distance between the sensor and the cutting edge is approximately 0.9 mm. The upper right inset

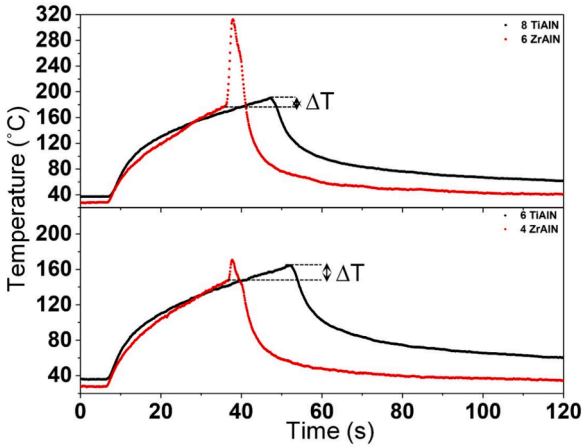

Fig. 8. Comparison of temperature profiles for TiAlN and ZrAlN sensor systems. The cutting conditions are as follows: cutting conditions 6 Table 2 – bottom plots; cutting conditions 8 Table 2 – top plots. The lathe's rotational speed was increased during ZrAlN sensor testing to maintain similar cutting speeds.

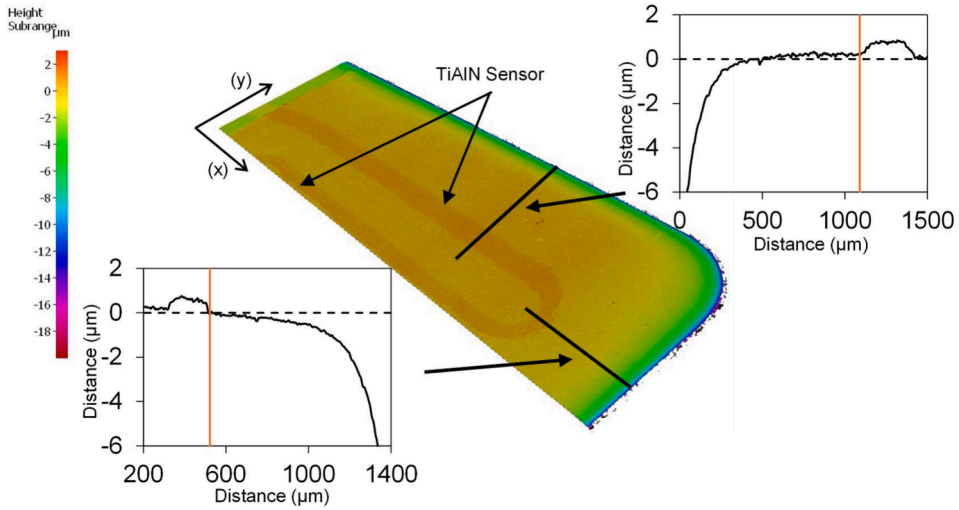

Fig. 9. 3D surface analysis of the cutting tool near the cutting edge, with the TiAlN as the temperature sensor. Insets showing the 2D profiles corresponding to the distance from the sensor to the cutting edge, where the red line assigns the edge of the sensor location. (For interpretation of the references to color in this figure legend, the reader is referred to the web version of this article.)

displays a similar profile but along the y-axis. The y distance between the sensor and the cutting edge is approximately 1.1 mm. The distances between the sensor and the cutting edge are slightly different from those shown in Fig. 2, which is expected due to the manual positioning of the shadow masks [16].

Fig. 10 presents the 3D color profile of the rake surface of the cutting tools containing TiAlN (Fig. 10(a)) and ZrAlN (Fig. 10(b)) sensors after performing the cutting tests. For the tool with the TiAlN sensor, three distinct types of wear are observed: notch wear, abrasive wear, and crater wear. The notch wear is localized beyond the contact length (equivalent to the chip width), approximately 2.8 mm for this cutting edge angle type, and a 2 mm depth of cut. This wear type is likely promoted by the sliding edge of long chips curling to the left side of the tool holder, meaning that localized material is removed due to high stresses and temperatures. The chip evacuation can be observed in the Supplementary Video Materials. Abrasive wear, the most predominant on the rake surface, results from the frictional contact between the workpiece material and the cutting edge during chip formation. The localized color index highlights the extent of the abrasive wear and shows a “stair” effect in the multilayer coating, progressively exposing the substrate. A combination of abrasion and diffusion mechanisms at the tool-chip interface causes the crater wear. Abrasion gradually removes the coating, exposing the substrate where diffusion of Co and C from the WC-Co into the chip occurs, further weakening the edge strength. This type of wear occurs at high temperatures [8,24] and is probably due to the high cutting speeds employed, namely the cutting conditions 10 (see Table 2). Moura et al. [8] realized that diffusion was the principal wear cause in carbide tools during titanium machining at high cutting speeds. Zhuang et al. [24] further confirmed the effect of the temperature by testifying that 800 °C is the threshold temperature to initiate the crater wear. The crater depth measured (~40 µm) is well within the permissible wear limits defined by ISO3685:1993, suggesting that the tool could perform additional cutting operations.

Another significant aspect revealed in Fig. 10(a) is the distance from the sensor to the worn zone; the sensor is approximately 680 µm from the crater center, where the highest temperatures are typically developed [24]. As discussed earlier, this positioning helps protect the sensor but limits the exact cutting temperature evaluation. The maximum temperature recorded (210 °C at a cutting speed of 80 m/min) reflects this limitation. To overcome the current constraints, we plan to explore techniques like laser-trimmed metal shadow masks. We believe this approach will enable us to position sensors closer to the cutting zone, allowing a more accurate measurement of the cutting temperatures. This improvement will enhance the sensors’ effectiveness for industrial applications.

Fig. 10(b) shows the cutting-edge of the tool with the ZrAlN as the temperature sensor. The abrasive wear extends far beyond the cutting edge length for the 2 mm depth of cut, impaired by the uncontrolled a_p experienced in Fig. 7. Given the length of the cutting edge exposed, it is possible to conclude that at a cutting temperature of 320 °C (see Fig. 7(b)) the depth of cut would be close to 8 mm. Additionally, chipping spots are detected, likely caused by the curling of the chip against the tool surface, which may suggest a brittle fracture of the protective coating. As this tool underwent fewer experiments, it exhibits less overall wear than the tool analyzed in Fig. 10(a), as expected. The distances from the sensor to the cutting edge are approximately 1.2 mm (x) and 1.0 mm (y), slightly different from the distances measured for the TiAlN sensor. These differences might introduce variability in temperature comparison between the sensors, as experienced in Fig. 8. Thus, the precise position of the sensor is essential for acquiring the actual cutting temperatures and conducting comparative analysis.

4. Conclusions

This study integrates traditional wear-resistant materials as temperature sensors into cutting tools, representing a significant

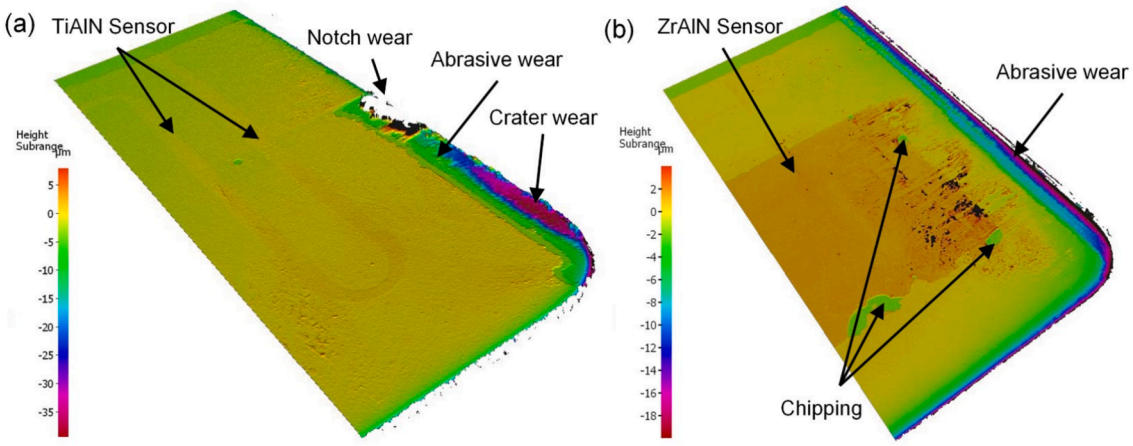

Fig. 10. 3D surface analysis of the cutting tool near the cutting edge after the cutting experiments: (a) surface 3D color profile for the cutting tool with TiAlN sensor, indicating notch wear, abrasive wear, and crater wear; (b) surface 3D color profile for the cutting tool with ZrAlN sensor, showing abrasive wear and chipping.

advancement in TCM by temperature, particularly for cutting titanium alloys. Multilayer coatings integrating TiAlN and ZrAlN temperature sensors were deposited on cutting inserts and calibrated up to 750 °C. The TiAlN and ZrAlN sensors exhibited β sensitivities of 108 and 950 K, respectively. The calibration process using the β function was admissible up to 400 °C; however, above that temperature, a sharp increase in the sensor's sensitivity undermined its utilization for the entire temperature range. This behavior was attributed to the effect of temperature on the insulation properties of the multilayer coating.

Both sensors were able to capture the essential thermal dynamics of the cutting process, but the selection between TiAlN and ZrAlN should consider factors such as sensitivity, calibration fit, or design. The cutting temperature is mainly affected by the cutting speed and depth of cut rather than by the feed rate, which emphasizes the need for optimizing the former variables for effective temperature control. Additionally, cooling significantly reduces cutting temperatures, proving more effective than adjusting V_c or a_p. The post-cutting surface analysis revealed the appearance of crater wear, suggesting that the positioning of the sensors plays a crucial role in accurate temperature measurement, as the maximum temperature captured was only 210 °C. Sensors placed too far from the cutting edge may not capture the peak temperatures.

Last, this research attempted to bridge the gap between laboratory experimentation and industrial temperature measurement applications by offering a practical solution for integrating smart cutting tools into traditional tool holders. Real-time wireless temperature monitoring improves machining processes by facilitating machine-to-tool communication. This alignment with Industry 4.0 goals allows for real-time adjustments to cutting conditions, contributing to increased efficiency and reduced operational costs. Nevertheless, future work must focus on improving the electrical insulation properties of the multilayer coating, refining shadow masks, and sensor positioning.

CRediT authorship contribution statement

Bruno Martins: Writing – original draft, Visualization, Investigation. **Carlos Patacas:** Visualization, Investigation. **Albano Cavaleiro:** Writing – review & editing, Validation, Supervision, Conceptualization. **Pedro Faia:** Writing – review & editing, Investigation. **Filipe Fernandes:** Writing – review & editing, Validation, Supervision, Conceptualization.

Declaration of competing interest

The authors declare that they have no known competing financial interests or personal relationships that could have appeared to influence the work reported in this paper.

Acknowledgements

This research is sponsored by national funds: Soft4Sense project "Smart Surfaces for Reliable Tooling Integration" (reference: POCI-01-0247-FEDER-045921), co-financed by the European Regional Development Fund, through Portugal 2020 (PT2020), by the Competitiveness and Internationalization Operational Programme (COMPETE 2020) and Foundation for Science and Technology (FCT). This research is also sponsored by national funds through FCT, under projects UIDB/00285/2020 and LA/P/0112/2020. The authors also express their gratitude towards the PRR Drivolution – Factory of the Future Model (reference: C644913740-00000022) for financial support and extend their appreciation to Ricardo Alexandre from Inovatools Portugal Unip. Lda for providing technical support.

Appendix A. Supplementary data

Supplementary data to this article can be found online at https://doi.org/10.1016/j.ymssp.2025.112444.

Data availability

Data will be made available on request.

References

[1] X. Li, X. Liu, C. Yue, S.Y. Liang, L. Wang, Systematic review on tool breakage monitoring techniques in machining operations, Int. J. Mach. Tools Manuf. 176 (2022) 103882, https://doi.org/10.1016/j.ijmachtools.2022.103882.

[2] R. Wang, Q. Song, Y. Peng, P. Jin, Z. Liu, Z. Liu, A milling tool wear monitoring method with sensing generalization capability, J. Manuf. Syst. 68 (2023) 25–41, https://doi.org/10.1016/j.jmsy.2023.02.017.

[3] J. Weng, J. Saelzer, S. Berger, K. Zhuang, A. Bagherzadeh, E. Budak, D. Biermann, Analytical and experimental investigations of rake face temperature considering temperature-dependent thermal properties, J. Mater. Process. Technol. 314 (2023) 117905, https://doi.org/10.1016/j.jmatprotec.2023.117905.

[4] S. Huang, B. Tao, J. Li, Y. Fan, Z. Yin, Estimation of the time and space-dependent heat flux distribution at the tool-chip interface during turning using an inverse method and thin film thermocouples measurement, Int. J. Adv. Manuf. Technol. 99 (2018) 1531–1543, https://doi.org/10.1007/s00170-018-2585-6.

[5] W. Liu, G. Li, Z. Shao, X. Wu, G. Ma, F. Wang, Advance in experimental research on cutting temperature of titanium alloys, Int. J. Adv. Manuf. Technol. 126 (2023) 1827–1844, https://doi.org/10.1007/s00170-023-11263-x.

[6] Y. Lian, X. Chen, T. Zhang, C. Liu, L. Lin, F. Lin, Y. Li, Y. Chen, M. Zhang, W. Zhou, Temperature measurement performance of thin-film thermocouple cutting tool in turning titanium alloy, Ceram. Int. 49 (2022) 2250–2261, https://doi.org/10.1016/j.ceramint.2022.09.193.

[7] T. Li, T. Shi, Z. Tang, G. Liao, J. Han, J. Duan, Temperature monitoring of the tool-chip interface for PCBN tools using built-in thin-film thermocouples in turning of titanium alloy, J. Mater. Process. Technol. 275 (2019) 116376, https://doi.org/10.1016/j.jmatprotec.2019.116376.

[8] R.R. Moura, M.B. da Silva, Á.R. Machado, W.F. Sales, The effect of application of cutting fluid with solid lubricant in suspension during cutting of Ti-6Al-4V alloy, Wear 332–333 (2015) 762–771, https://doi.org/10.1016/j.wear.2015.02.051.

[9] S. Huang, B. Tao, J. Li, Y. Fan, Z. Yin, On-line estimation of the tool-chip interface temperature field during turning using a sequential inverse method, Int. J. Adv. Manuf. Technol. (2018).

[10] J. Li, B. Tao, S. Huang, Z. Yin, Built-in thin film thermocouples in surface textures of cemented carbide tools for cutting temperature measurement, Sensors Actuators, A Phys. 279 (2018) 663–670, https://doi.org/10.1016/j.sna.2018.07.017.

[11] Y. Niu, H. Dong, H. Wang, T. Liu, X. Li, Q. Tan, J. Xiong, Design and performance evaluation of an all-ceramic high-temperature test sensor, J. Alloys Compd. 938 (2023) 168561, https://doi.org/10.1016/j.jallcom.2022.168561.

[12] J. Li, B. Tao, S. Huang, Z. Yin, Cutting tools embedded with thin film thermocouples vertically to the rake face for temperature measurement, Sensors Actuators, A Phys. 296 (2019) 392–399, https://doi.org/10.1016/j.sna.2019.07.043.

[13] B. Guimarães, C. Fernandes, D. Figueiredo, F. Silva, M. Miranda, Cutting temperature measurement and prediction in machining processes: comprehensive review and future perspectives, Int. J. Adv. Manuf. Technol. (2022). https://doi.org/https://doi.org/10.1007/s00170-022-08957-z.

[14] B. Martins, C. Patacas, A. Cavaleiro, P. Faia, O. Bondarchuk, F. Fernandes, Electrical properties and thermistor behavior of TiAlN thin films deposited by combinatorial sputtering, Surf. Coat. Technol. 464 (2023) 129545, https://doi.org/10.1016/j.surfcoat.2023.129545.

[15] B. Martins, C. Patacas, A. Cavaleiro, P. Faia, O. Bondarchuk, F. Fernandes, Can ZrAlN thin films be used as thermistor sensors for temperature assessment ?,, J. Sci. Adv. Mater. Devices. 9 (2024) 100676, https://doi.org/10.1016/j.jsamd.2024.100676.

[16] B. Martins, C. Patacas, A. Cavaleiro, P. Faia, F. Zorro, E. Carbo-argibay, P.J. Ferreira, F. Fernandes, Expanding the applications of the wear-resistant titanium aluminum nitride thin-film to include temperature sensing, J. Sci. Adv. Mater. Devices. 9 (2024), https://doi.org/10.1016/j.jsamd.2024.100716.

[17] A. Feteira, Negative temperature coefficient resistance (NTCR) ceramic thermistors: An industrial perspective, J. Am. Ceram. Soc. 92 (2009) 967–983, https://doi.org/10.1111/j.1551-2916.2009.02990.x.

[18] S. Jagtap, S. Rane, S. Gosavi, D. Amalnerkar, Study on I-V characteristics of lead free NTC thick film thermistor for self heating application, Microelectron. Eng. 88 (2011) 82–86, https://doi.org/10.1016/j.mee.2010.08.025.

[19] Q. Wang, W. Kong, J.C. Yao, A. Chang, Fabrication and electrical properties of the fast response Mn1.2Co1.5Ni0.3O4 miniature NTC chip thermistors, Ceram. Int. 45 (2019) 378–383, https://doi.org/10.1016/j.ceramint.2018.09.177.

[20] M. Gillinger, M. Schneider, A. Bittner, P. Nicolay, U. Schmid, Impact of annealing temperature on the mechanical and electrical properties of sputtered aluminum nitride thin films, J. Appl. Phys. 117 (2015), https://doi.org/10.1063/1.4907208.

[21] M. Schneider, A. Bittner, U. Schmid, Impact of film thickness on the temperature-activated leakage current behavior of sputtered aluminum nitride thin films, Sensors Actuators, A Phys. 224 (2015) 177–184, https://doi.org/10.1016/j.sna.2015.01.032.

[22] H. Liu, X. Mao, S. Jiang, Effect of thermally grown Al2O3 on electrical insulation properties of thin film sensors for high temperature environments, Sensors Actuators A Phys. 331 (2021) 113033, https://doi.org/10.1016/j.sna.2021.113033.

[23] J. Zhao, Z. Liu, B. Wang, J. Hu, Y. Wan, Tool coating effects on cutting temperature during metal cutting processes: Comprehensive review and future research directions, Mech. Syst. Signal Process. 150 (2021), https://doi.org/10.1016/j.ymssp.2020.107302.

[24] K. Zhuang, M. Li, F. Lin, C. Hu, J. Weng, Z. Gao, C. Wu, Crater wear prediction in turning Ti6Al4V considering cutting temperature effect, Int. J. Adv. Manuf. Technol. 121 (2022) 6763–6781, https://doi.org/10.1007/s00170-022-09773-1.